

# 3-D CFD MODELING OF GAS TURBINE COMBUSTOR-INTEGRAL BLEED FLOW INTERACTION

D. Y. Chen

and

R. S. Reynolds

AlliedSignal Engines  
P.O. Box 52180  
Phoenix, AZ 85072-2180

## ABSTRACT

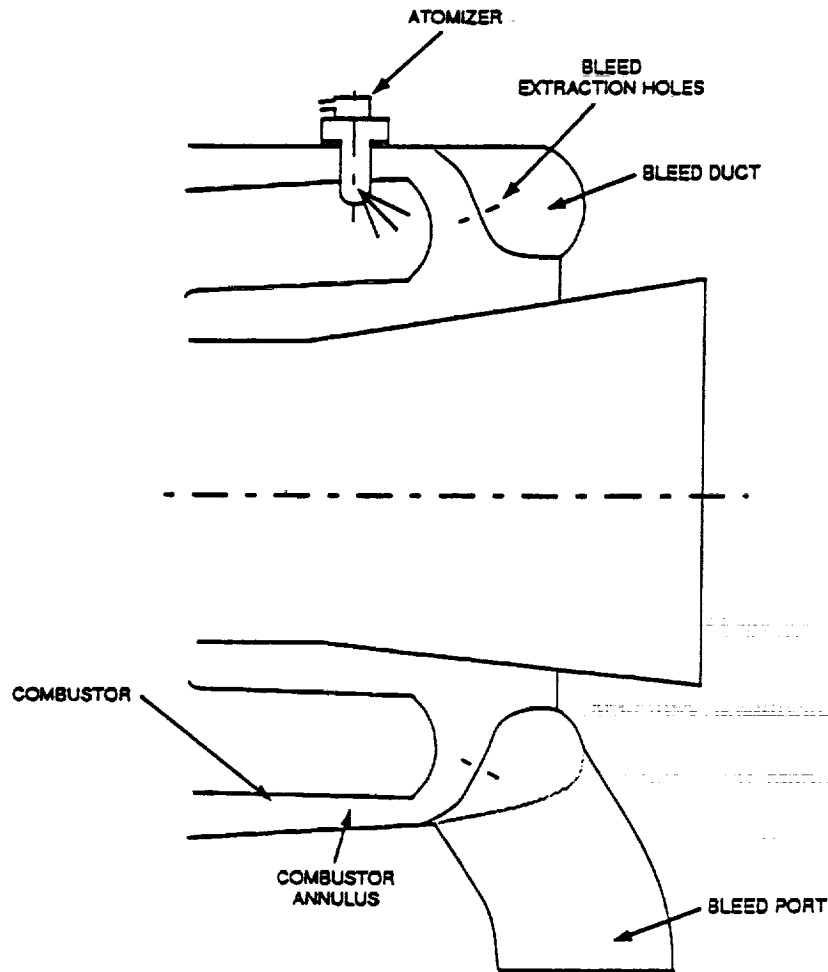
An advanced 3-D Computational Fluid Dynamics (CFD) model was developed to analyze the flow interaction between a gas turbine combustor and an integral bleed plenum. In this model, the elliptic governing equations of continuity, momentum and the k- $\epsilon$  turbulence model were solved on a boundary-fitted, curvilinear, orthogonal grid system. The model was first validated against test data from public literature and then applied to a gas turbine combustor with integral bleed. The model predictions agreed well with data from combustor rig testing. The model predictions also indicated strong flow interaction between the combustor and the integral bleed. Integral bleed flow distribution was found to have a great effect on the pressure distribution around the gas turbine combustor.

## INTRODUCTION

The onboard gas turbine auxiliary power unit (APU) generally is designed to deliver bleed air either from a basic APU or from a separate compressor. The bleed air supplied by the APU normally is used for starting the main engines and operating the air-cycle air conditioning and pressurization system. On the direct-bleed APU (also called integral-bleed APU), bleed air is extracted from a point between the compressor and combustor, as shown in Figure 1, and is routed to the airplane pneumatic system via a bleed valve attached to a port on the turbine plenum.

The bleed air extraction from the turbine plenum has long been recognized among APU combustor designers to have a significant effect on combustor performance. However, knowledge in this field is limited and has been acquired only as a result of rig or engine testings. No theoretical modeling has been conducted and reported in the literature. The purpose of this study is to do a comprehensive theoretical investigation into the flow interaction between a gas turbine combustor and an integral bleed plenum. Findings from this study should prove useful in the design and development of a gas turbine combustor with integral bleed.

The flow interaction between a gas turbine combustor and an integral bleed is fully three-dimensional and extremely complicated. To do 3-D Computational Fluid Dynamics (CFD) modeling of this complex flow interaction using a cylindrical grid system requires a huge number of grid nodes and complex treatment of wall boundary conditions. Recently, a large variety of numerical grid generation methods [1] have been developed to simplify wall boundary condition treatment for any complex flow geometry. These methods can generate either orthogonal or non-orthogonal boundary-fitted grid systems for any complex flow geometry. In this study, a boundary-fitted, curvilinear, orthogonal grid system is used for the two-dimensional (x,y) plane and the angular (z)



GC11476-1

**Figure 1. A Typical Gas Turbine Combustor with Integral Bleed.**

dimension is considered as a body of revolution. The choice of a curvilinear orthogonal grid system in the present flow modeling is motivated by easier wall boundary condition treatment, inclusion of most of the grid nodes in the computational domain, and no extra terms of cross-derivative appearing in the transformed governing equations.

### ORTHOGONAL GRID GENERATION

As mentioned above, the flow geometry of a gas turbine combustor with integral bleed is quite complex for 3-D CFD modeling. A boundary-fitted, curvilinear, orthogonal grid system is therefore used here. The orthogonal grid system used in this study was obtained numerically based on the following 2-D orthogonal grid generation model:

Governing Equations:

$$\xi_{xx} + \xi_{yy} = P \quad (1)$$

$$\eta_{xx} + \eta_{yy} = Q \quad (2)$$

Boundary Conditions:

$$BC1: \xi_x \eta_x + \xi_y \eta_y = 0; F_1(\xi, \eta) = 0 \quad (3)$$

$$BC2: \xi_x \eta_x + \xi_y \eta_y = 0; F_2(\xi, \eta) = 0 \quad (4)$$

$$BC3: \xi_x \eta_x + \xi_y \eta_y = 0; F_3(\xi, \eta) = 0 \quad (5)$$

$$BC4: \xi_x \eta_x + \xi_y \eta_y = 0; F_4(\xi, \eta) = 0 \quad (6)$$

where  $(x,y)$  are the Cartesian coordinates of the grid points in the physical plane, as shown in Figure 2, and  $(\xi, \eta)$  are the coordinates of the corresponding grid points in the transformed plane. The control functions  $P$  and  $Q$  in equations (1) and (2) are used to concentrate grid lines as desired. The function  $F$  denotes user-specified boundary curves. In order to facilitate numerical solution for the above equations (1) to (6), they were transformed into the following equations:

Governing Equations:

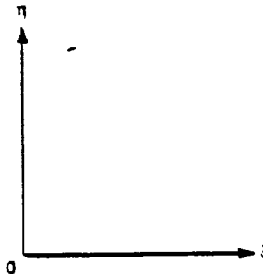
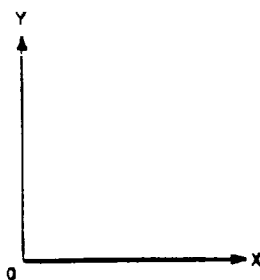
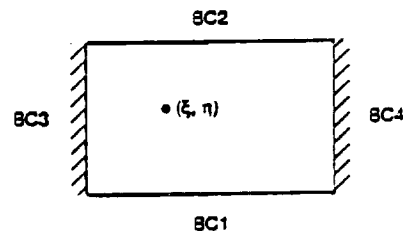
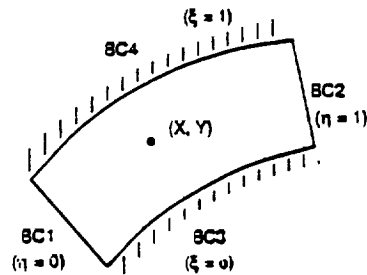
$$\alpha x_{\xi\xi} - 2\beta x_{\xi\eta} + \gamma x_{\eta\eta} = -J^2(x_{\xi}P + x_{\eta}Q) \quad (1a)$$

$$\alpha y_{\xi\xi} - 2\beta y_{\xi\eta} + \gamma y_{\eta\eta} = -J^2(y_{\xi}P + y_{\eta}Q) \quad (2a)$$

PHYSICAL PLANE



TRANSFORMED PLANE



GC11478-2A

Figure 2. Coordinate Transformation.

where

$$\alpha = (x_\eta^2 + y_\eta^2)$$

$$\beta = (x_\xi x_\eta + y_\xi y_\eta)$$

$$\gamma = (x_\xi^2 + y_\xi^2)$$

$$J = x_\xi y_\eta - x_\eta y_\xi$$

Boundary Conditions:

$$BC1: x_\xi x_\eta + y_\xi y_\eta = 0 ; G_1(x, y) = 0 \quad (3a)$$

$$BC2: x_\xi x_\eta + y_\xi y_\eta = 0 ; G_2(x, y) = 0 \quad (4a)$$

$$BC3: x_\xi x_\eta + y_\xi y_\eta = 0 ; G_3(x, y) = 0 \quad (5a)$$

$$BC4: x_\xi x_\eta + y_\xi y_\eta = 0 ; G_4(x, y) = 0 \quad (6a)$$

These transformed equations are solved numerically using a finite difference technique. This grid generation model only generates a boundary-fitted, curvilinear, orthogonal grid system in two dimensions. The present flow calculation requires a 3-D orthogonal grid system, obtained by rotating this 2-D orthogonal grid system about an axis in the same plane. Using this approach, a typical 3-D grid system for the combustor with integral bleed flow calculation is shown in Figure 3.

### MATHEMATICAL MODEL

The transport equations for a 3-D incompressible turbulent flow can be written as

$$\frac{\partial}{\partial x} (\rho u \phi - \Gamma \frac{\partial \phi}{\partial x}) + \frac{\partial}{\partial y} (\rho v \phi - \Gamma \frac{\partial \phi}{\partial y}) + \frac{\partial}{\partial z} (\rho w \phi - \Gamma \frac{\partial \phi}{\partial z}) = S_\phi$$

where  $\phi$  represents a general variable,  $\rho$  is density,  $U$ ,  $V$ , and  $W$  are velocities,  $\Gamma$  is effective turbulent diffusivity, and  $S_\phi$  is the source term for variable  $\phi$ .

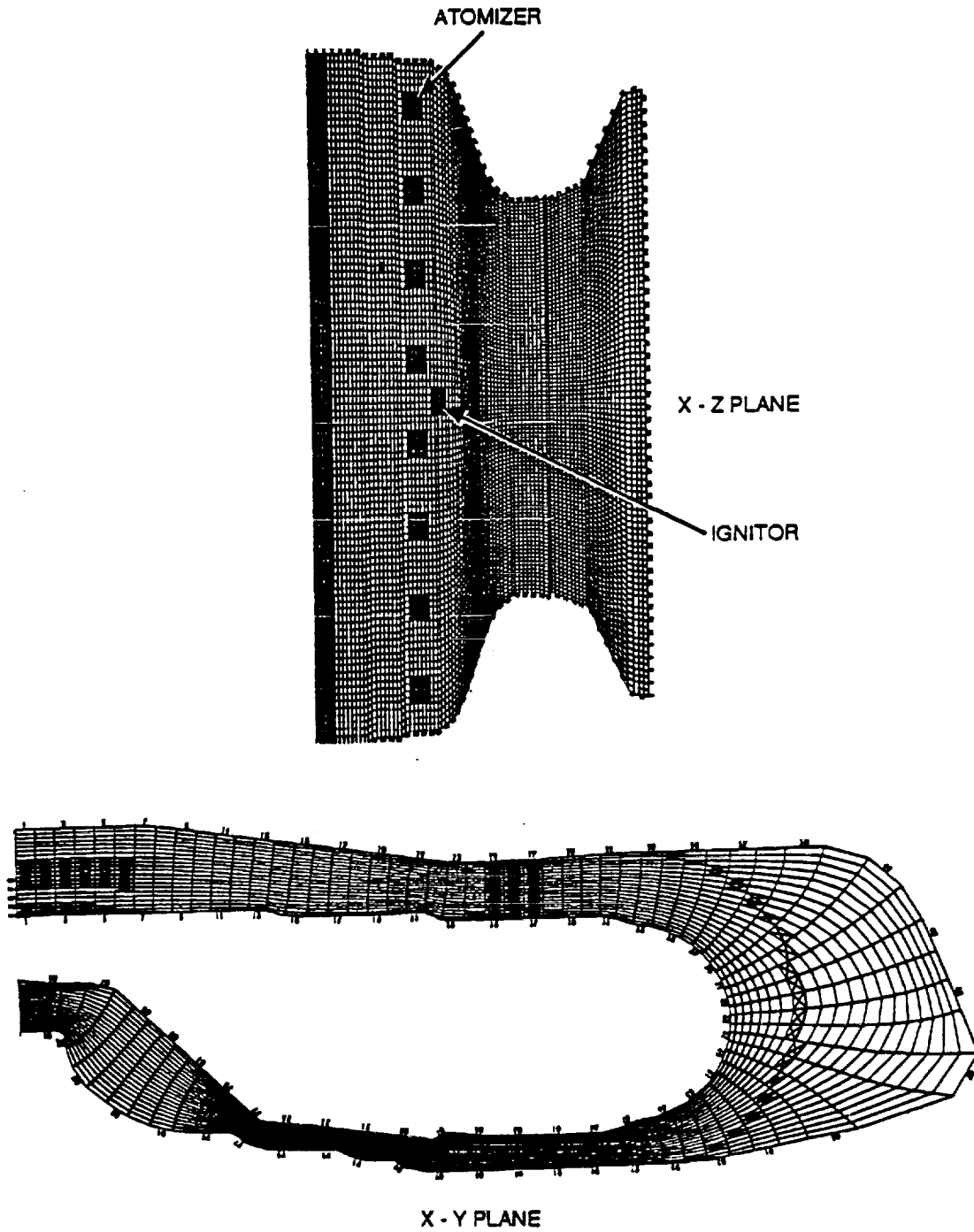
The above transport equations are given in Cartesian coordinates  $(x, y, z)$ . Prior to their numerical solution, these equations are transformed into general orthogonal coordinates  $(\xi, \eta, \zeta)$ . The resulting transport equations are expressed as follows:

$$\frac{\partial}{\partial \xi} (h_2 h_3 (\rho u \phi - \frac{\Gamma}{h_1} \frac{\partial \phi}{\partial \xi})) + \frac{\partial}{\partial \eta} (h_3 h_1 (\rho v \phi - \frac{\Gamma}{h_2} \frac{\partial \phi}{\partial \eta})) + \frac{\partial}{\partial \zeta} (h_1 h_2 (\rho w \phi - \frac{\Gamma}{h_3} \frac{\partial \phi}{\partial \zeta})) = h_1 h_2 h_3 S_\phi$$

where  $h$  represents scalar coefficients.

In order to solve the above partial differential equations governing the flow of fluid through a combustor annulus with integral bleed, boundary conditions must be specified at the appropriate locations. In the present study, the boundary conditions at the annulus inlet and the bleed duct exit are

provided from the engine cycle analysis, while the airflow through the various orifices in the combustor, as shown in Table 1, are calculated using a I-D annulus flow model.



GC11476-3

**Figure 3. A Typical Orthogonal Grid System for the Combustor with Integral Bleed Flow Calculation.**

**TABLE 1. AIRFLOW DISTRIBUTIONS AROUND THE COMBUSTOR**

	<b>OD</b>	<b>ID</b>
Primary Holes	4.28	9.90
Dilution Holes	5.59	5.69
Film Cooling	10.90	7.15
Dome Cooling	11.21	--
Bleed	42.01	--
Shroud Air	1.10	--
<u>Leakage</u>	<u>1.28</u>	<u>0.89</u>
<b>Total</b>	<b>76.37%</b>	<b>23.63%</b>

The solution of the curvilinear transport equations is accomplished using a finite volume, structured grid, sequential solution, numerical method. The differential equations are integrated over discrete volumes in the domain of interest using assumptions of linear and stepped profiles to obtain their numerical counterparts. Interaction between the convective and diffusive terms is handled numerically using Upwind Hybrid Differencing [2], while the coupling between the continuity and momentum equations is treated by the SIMPLER algorithm [3] and the turbulence closure is accomplished by the standard k-e model. At each iteration step, the set of linear equations is solved using the Whole Field Solver (WFS) routine of Przekwas [4]. The WFS has proven to be very efficient as it is formulated for structured grids and cyclic boundary conditions which are used in this analysis.

The use of orthogonal coordinate systems adds effort to the grid generation process, as numerical equations must be solved to determine the position of the coordinates in the physical space. It is also frequently the case that the shape of the domain is such that a completely orthogonal grid system cannot be generated and a certain amount of deviation from orthogonality must be tolerated. However, the benefits of this extra work are realized when the flow equations are solved. The terms associated with grid non-orthogonality are usually treated in an explicit manner and in situations of skewed control volumes, can be the same order of magnitude as the normal implicit convection and diffusion terms. As a result, convergence can be hindered. Orthogonal grids create a more implicit nature to the numerical equations and have inherently better convergence rates.

The combination of the SIMPLER algorithm and the orthogonal grid structure has proven to be extremely robust. In all but a very few situations, relaxation factors of 0.5 are used on all equations (except for pressure and the velocity correction which require 1.0 relaxation factors). Converged solutions using up to 400,000 cells have been obtained in the order of 750 iterations. At convergence, the sum of the absolute continuity error of all the control volumes, normalized by the total system flow rate, is less than 0.1 percent.

## NUMERICAL RESULTS

The predictions of the CFD model used in this study have been compared to numerous sets of experimental data found in the literature. In order to illustrate the predictive capability of the code, two such cases have been included below, both of which are 2-D flows. For these situations, the 3-D code was run with three circumferential planes.

The first case is from the experiment of Roback and Johnson [5] and consists of two coaxial flowing water jets that discharge into a confined region (illustrated in Figure 4). The inner jets are swirling while the outer are not. Velocity data was taken at several axial stations downstream of the jet discharge. Figure 5 shows the comparison of the predicted and measured axial, radial, and tangential velocity components respectively. The comparison is as good as should be expected considering the well known deficiencies of the k-e model for swirling flow and the uncertainty in the boundary conditions of the data.

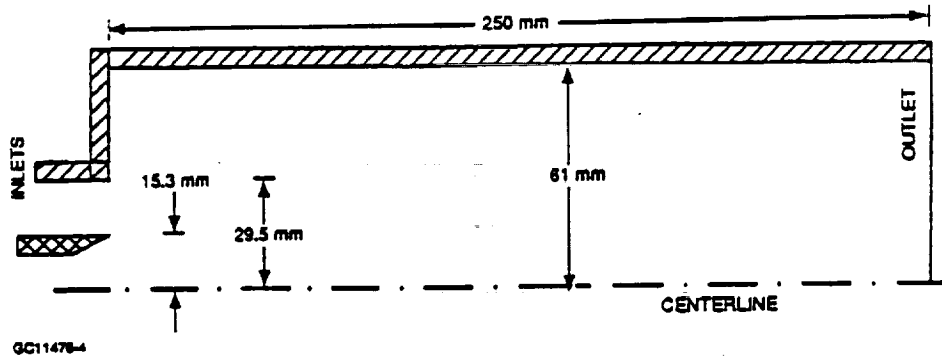


Figure 4. Axisymmetric Swirling Flow Geometry.

The second case described is that of Sovran and Klomp [6] and consists of a 6-degree wall annular diffuser with an area ratio of 1.955. The computed static pressure contours (Pascals) are shown in Figure 6. The experimental data for this case consist of the static pressure recovery coefficient,  $C_p$ . For the configuration analyzed, the measured  $C_p$  was 0.6 which should be compared to the value of 0.643 (7 percent high) calculated from the CFD model output, indicating reasonable accuracy in the pressure calculation methods used in the code.

After validation of the 3-D CFD model using experimental data found in the literature, the present model was then used to simulate complex external flow of a gas turbine combustor with integral bleed. The computed results using a grid system of 91x21x97 nodes, as shown in Figure 3, are discussed in the following:

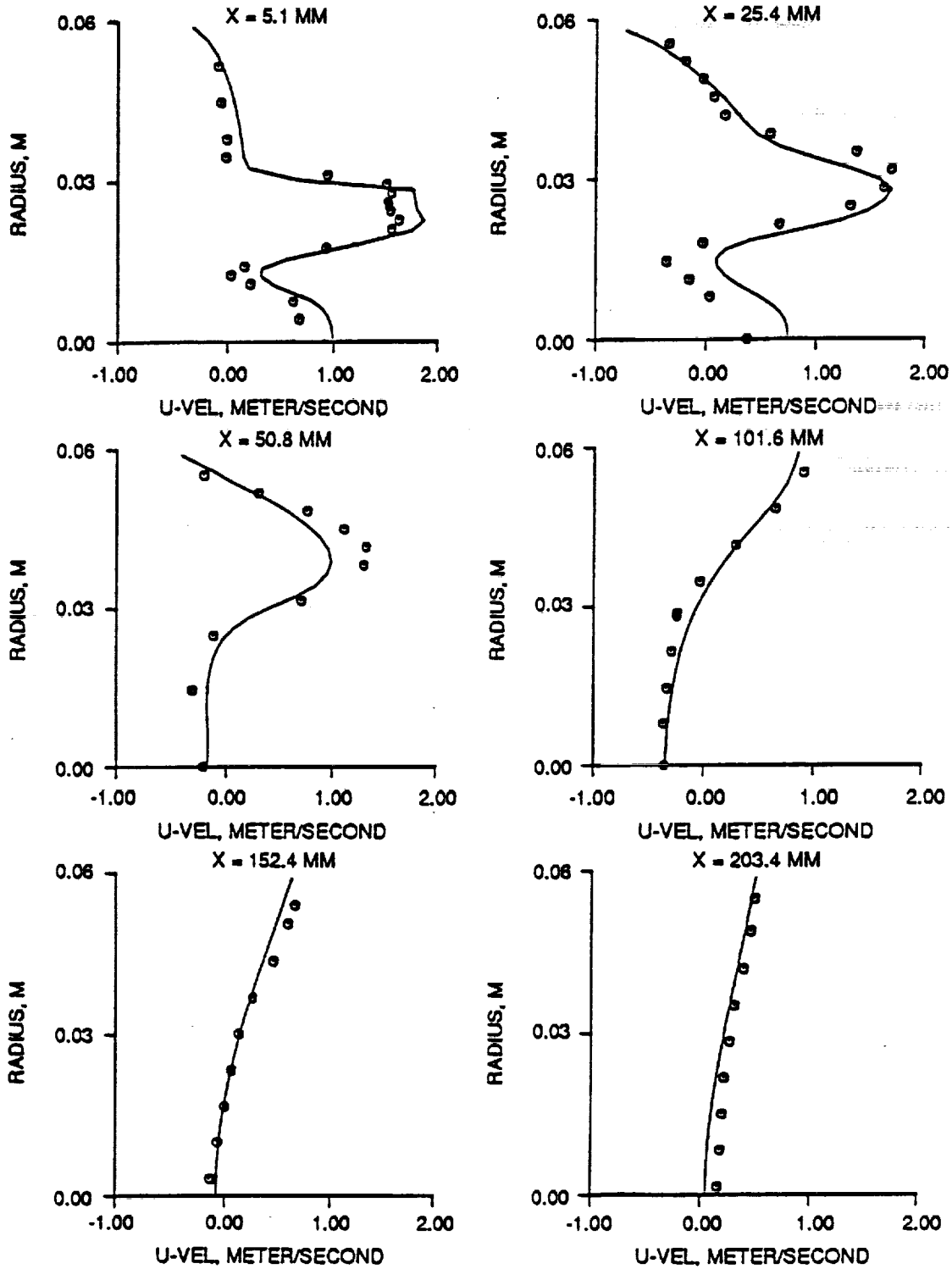
Figure 7 shows the predicted U-V velocity field at K-planes 1, 38, and 59. The predicted results illustrate a strong recirculation zone formed near the annulus inlet. The formation of this recirculation zone is due to the presence of a backward-facing step in the flow path. This recirculation zone has caused pressure loss near the combustor O.D. dilution holes. As a result, the dilution jet penetration will be reduced because of less pressure drop across dilution holes. Based on gas turbine combustor design experiences, inadequate dilution jet penetration usually cannot break up the hot gas regions efficiently and will result in high pattern factor at the combustor exit.

The predicted results, as shown in Figure 7, also illustrate non-uniform bleed air extraction from the turbine plenum. The bleed air extraction at K-plane 59, which is closer to bleed port (K-planes 61-65), is higher than that at K-plane 38. The non-uniform bleed air extraction indicates that the present integral bleed design has not been optimized and has caused some flow separations in the annulus. It is also interesting to note that bleed air enters the bleed duct like an impinged jet and creates a vortex pair in the duct.

Figure 8 shows the predicted U-W velocity field on the unwrapped surface of combustor liner. The predicted results indicate that a forward stagnation point, where the air is brought to rest with an accompanying rise in pressure, was formed upstream of a fuel atomizer or an ignitor. The predicted results also indicate that a strong wake was formed downstream of a fuel atomizer or an ignitor.

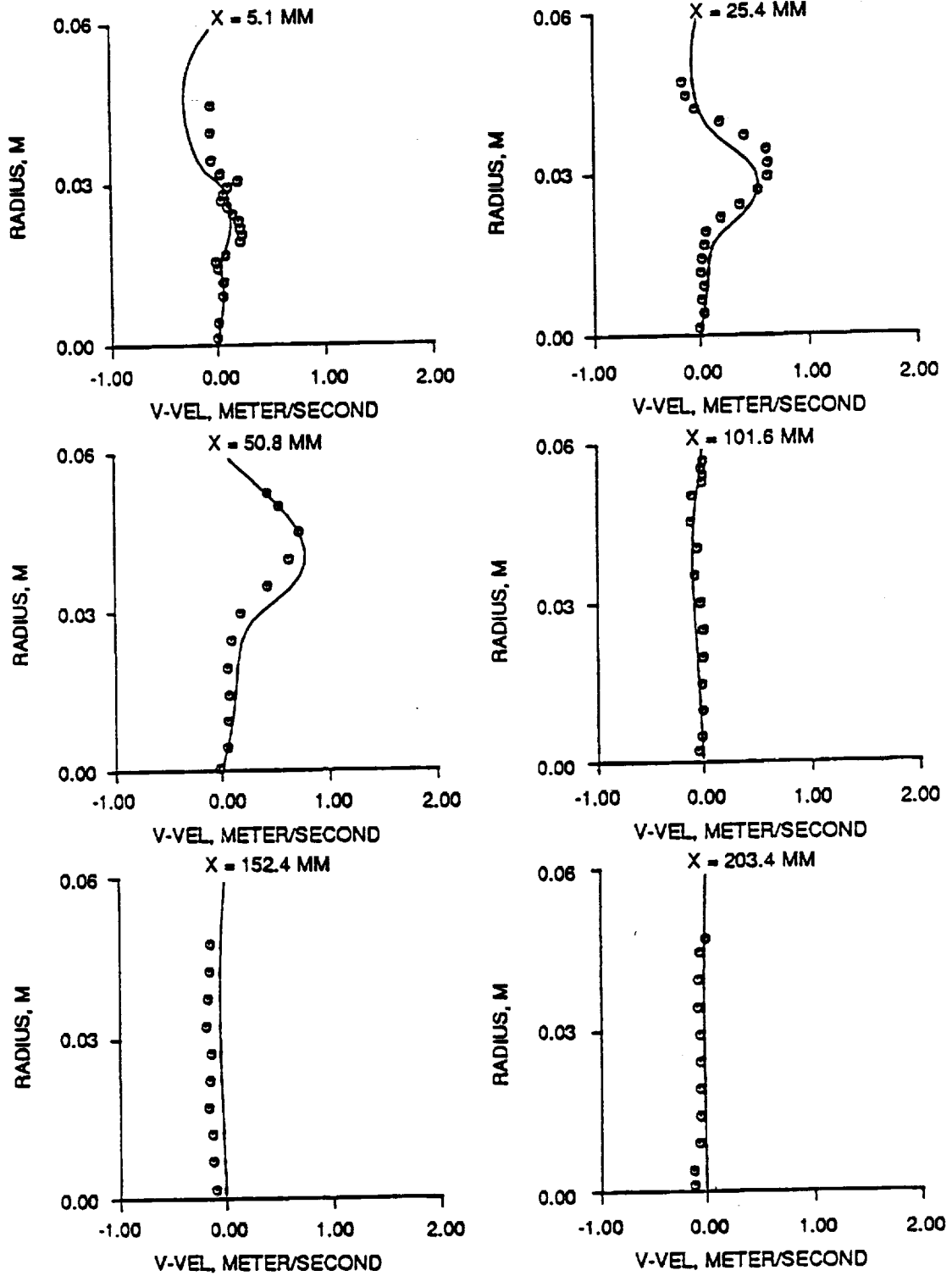
The presence of eight fuel atomizers and one ignitor has a profound effect on pressure distributions around the combustor liner. This can be seen in Figure 9, where the predicted static pressure distributions around the combustor liner is plotted using color graphics. In this figure, each fuel atomizer was found to be associated with a high pressure region upstream and a low pressure region downstream. The same pattern was observed for the ignitor. Figure 9 also shows non-uniform bleed extraction has a great effect on pressure distribution around the combustor liner. This is illustrated by results of non-uniform pressure distribution on the dome. Based on gas turbine combustor design experience, non-uniform pressure distribution around the combustor liner usually causes non-uniform airflow distribution and will result in hot and cold spots at the combustor exit.

Figure 10 shows the predicted static pressure distributions around the turbine plenum. The predicted results further illustrate that the presence of eight fuel atomizers and one ignitor has a



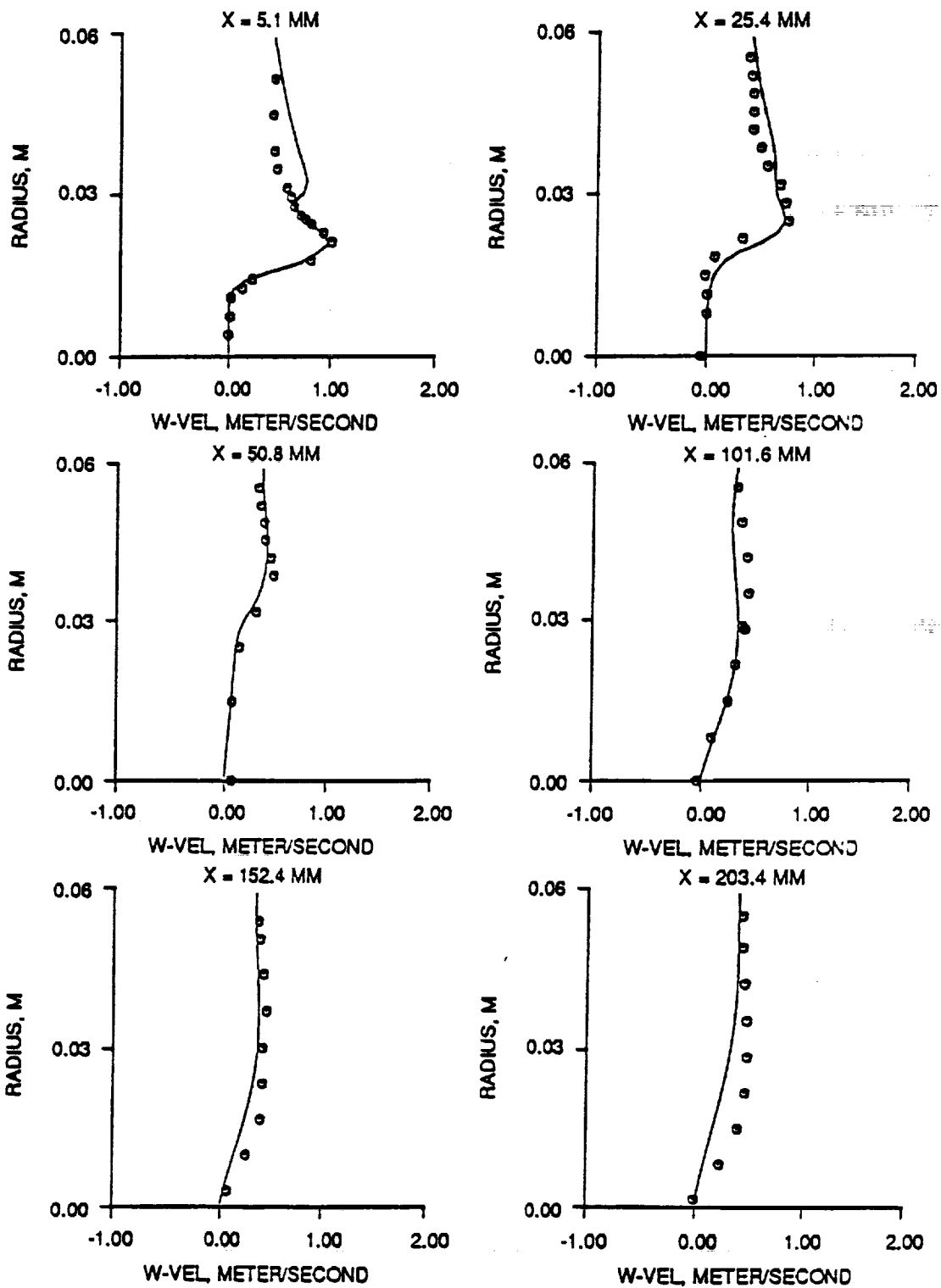
GC11476-5-1

Figure 5a. Comparison of Predictions and Measurements of Velocity Distributions for Confined Coaxial Jets.



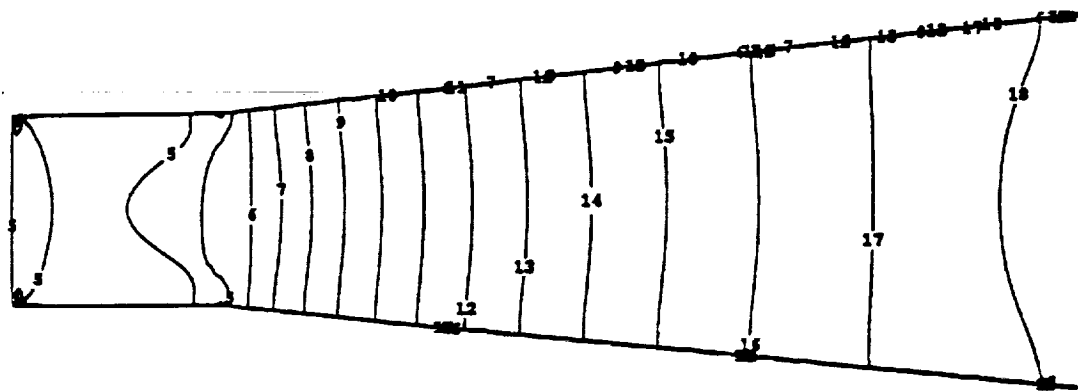
GC11476-5-2

Figure 5b. Comparison of Predictions and Measurements of Velocity Distributions for Confined Coaxial Jets.



GC11478-5-3

Figure 5c. Comparison of Predictions and Measurements of Velocity Distributions for Confined Coaxial Jets.



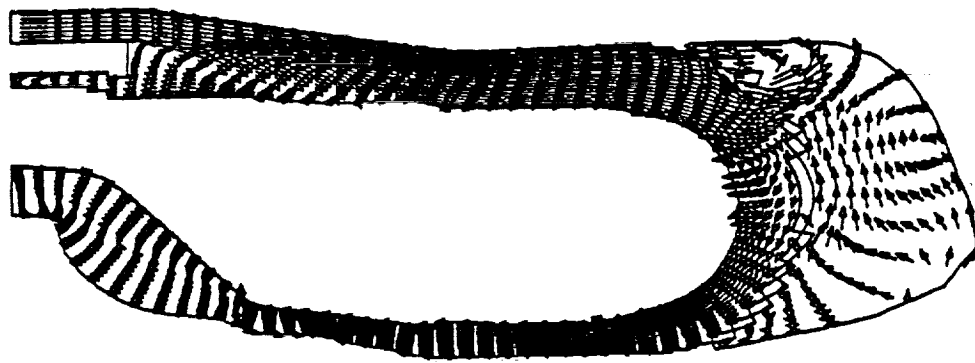
CONTOUR VALUE

1	-1200.0	11	1800.0
2	-900.0	12	2100.0
3	-600.0	13	2400.0
4	-300.0	14	2700.0
5	0.0	15	3000.0
6	300.0	16	3300.0
7	600.0	17	3600.0
8	900.0	18	3900.0
9	1200.0	19	4200.0
10	1500.0		

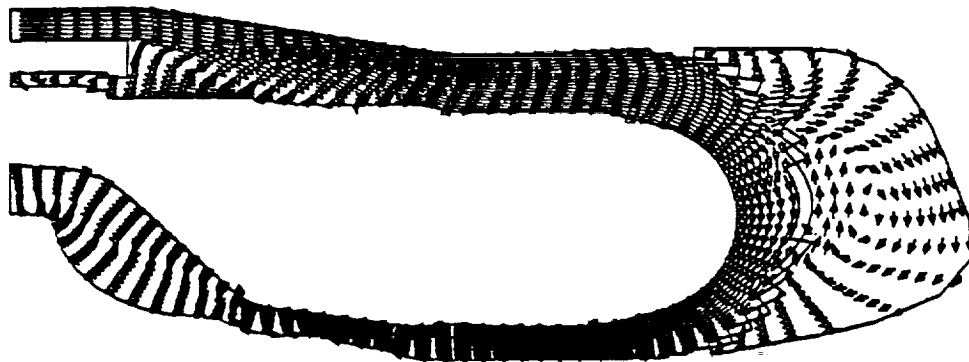


GC11478-8

Figure 6. Pressure Contours for Annular Diffuser.



K = 59



K = 38

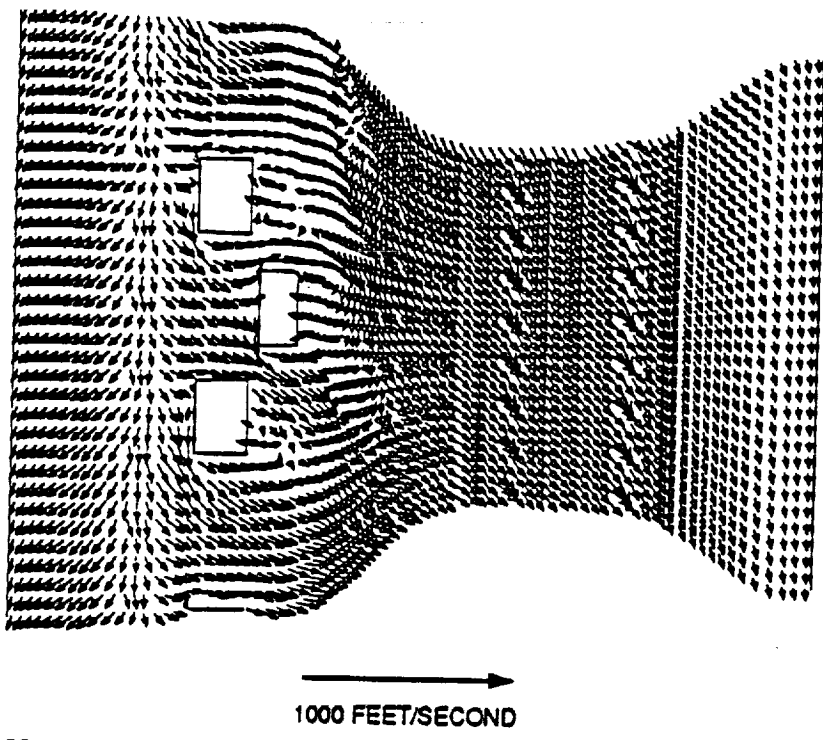
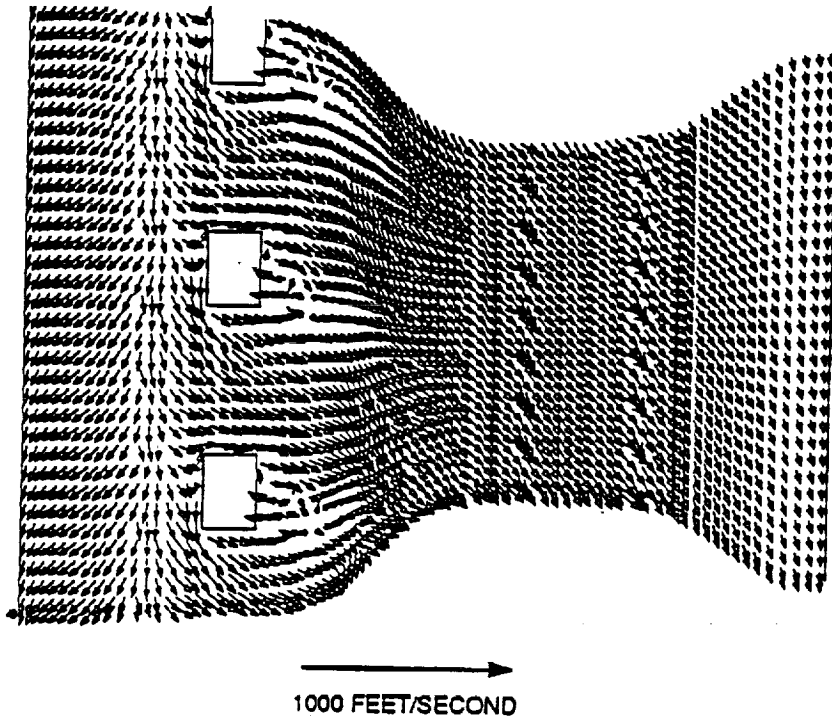


K = 1

→  
1000 FEET/SECOND

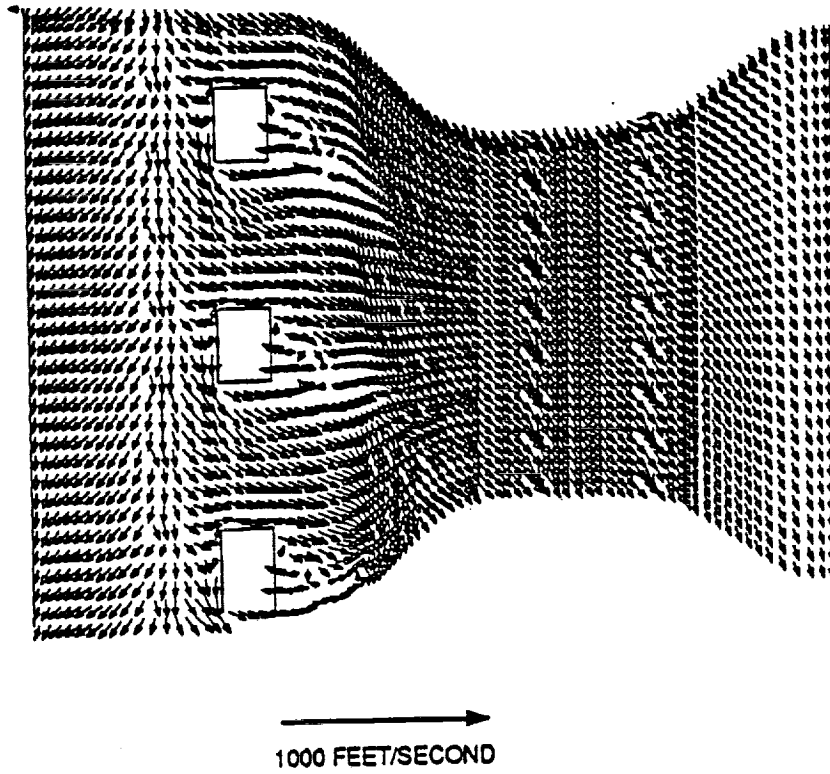
GC11478-7

Figure 7. Predicted U-V Velocity Field around Combustor.



GC11476-8-1

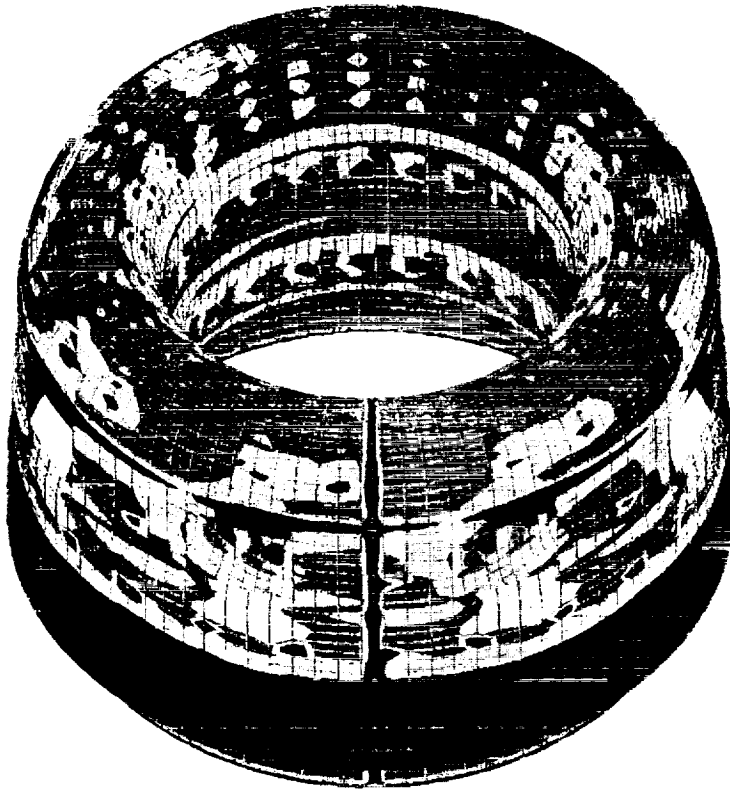
Figure 8a.b. Predicted U-W Velocity Field around Combustor.



GC11478-8-2

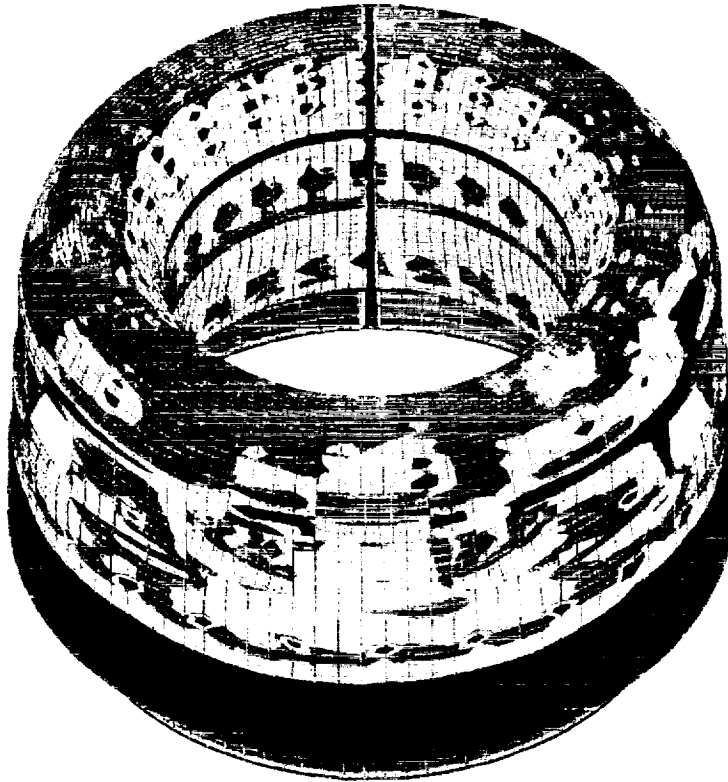
**Figure 8c. Predicted U-W Velocity Field around Combustor.**

STATIC PRESSURE (PSI)



(a)

STATIC PRESSURE (PSI)



(b)

74.0

73.8

73.6

73.4

73.2

73.0

72.8

72.6

72.4

72.2

72.0

71.8

71.6

71.4

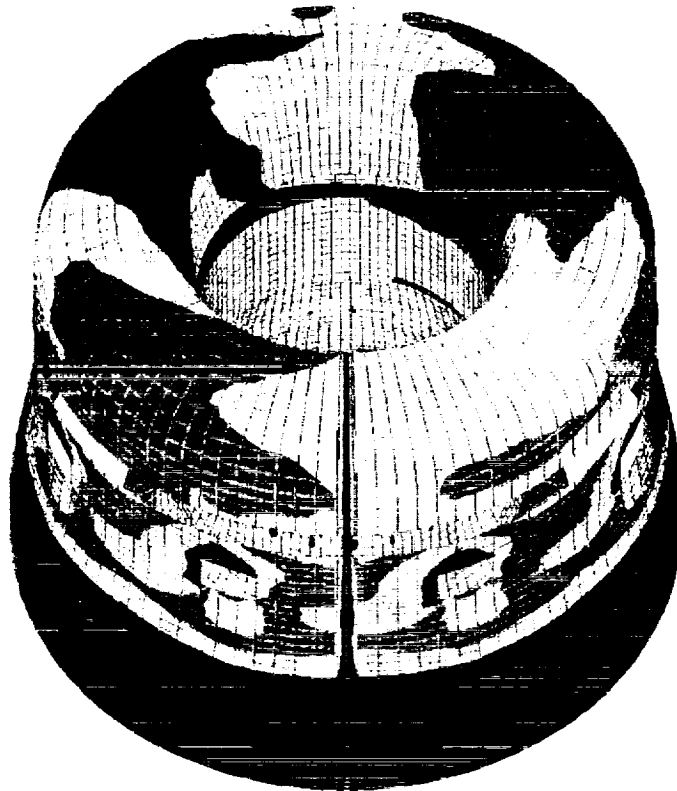
71.2

GB11476-9

Figure 9. Predicted Pressure Distributions around Combustor.

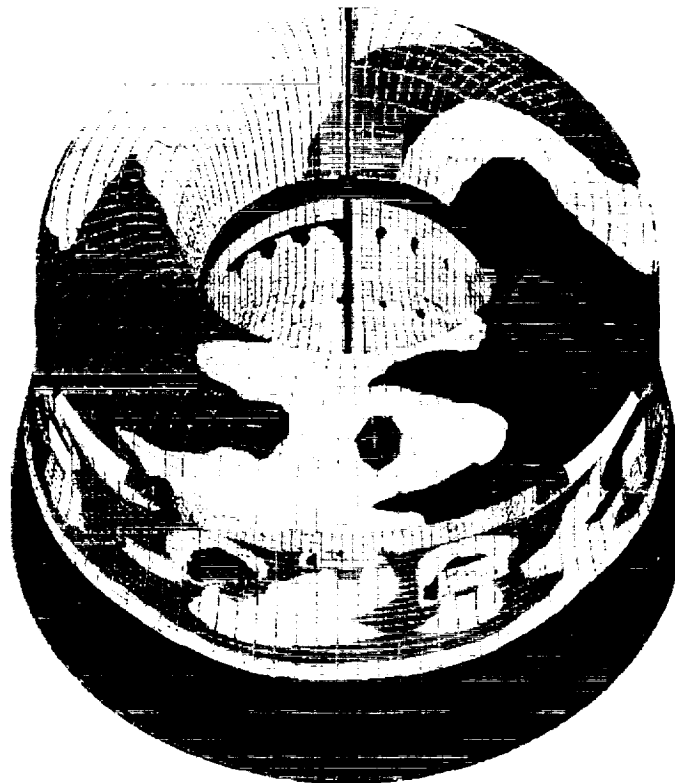


STATIC PRESSURE (PSI)

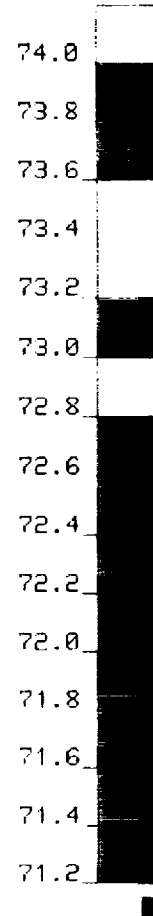


(a)

STATIC PRESSURE (PSI)



(b)



GB11476-10

Figure 10. Predicted Pressure Distributions around Turbine Plenum.

1. The first part of the document discusses the importance of maintaining accurate records of all transactions and activities. It emphasizes that this is crucial for ensuring transparency and accountability in the organization's operations.

2. The second part of the document outlines the various methods and tools used to collect and analyze data. It highlights the need for consistent data collection procedures and the use of advanced analytical techniques to derive meaningful insights from the data.

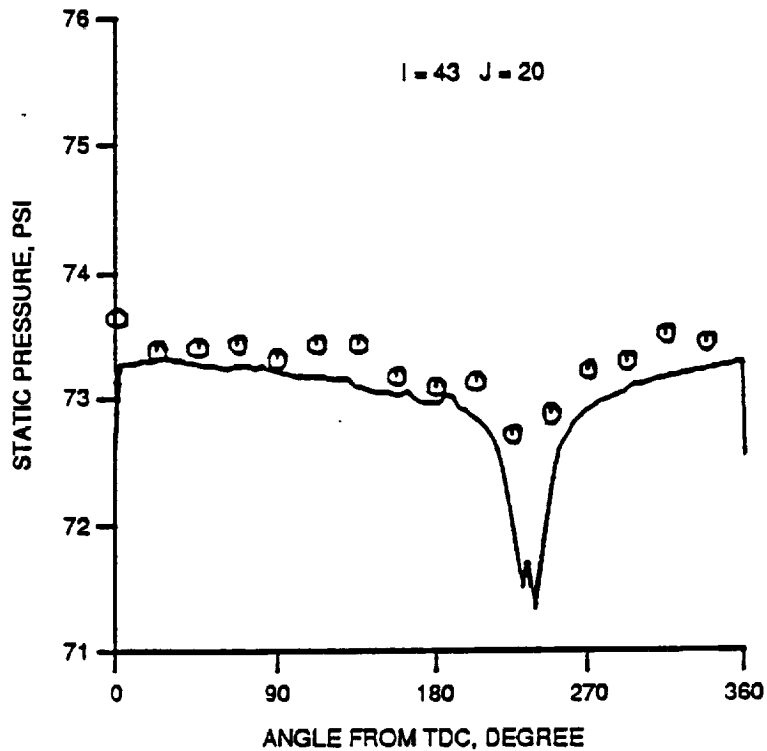
3. The third part of the document focuses on the role of technology in data management and analysis. It discusses how modern software solutions can streamline data collection, storage, and analysis processes, thereby improving efficiency and accuracy.

4. The fourth part of the document addresses the challenges associated with data management, such as data quality, security, and privacy. It provides strategies to mitigate these risks and ensure that the data remains reliable and secure throughout its lifecycle.

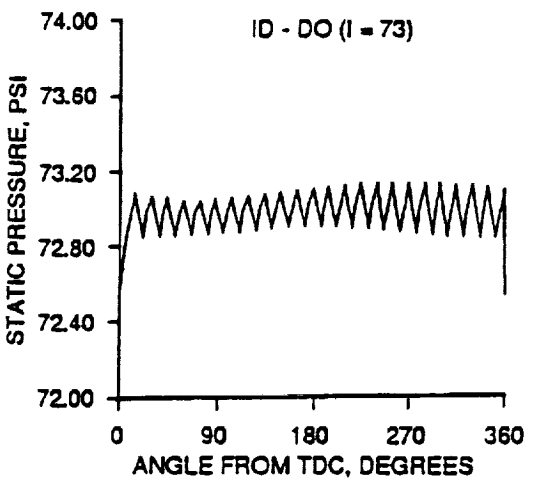
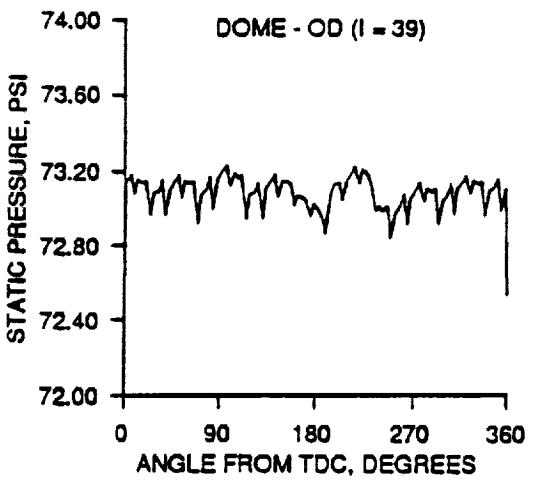
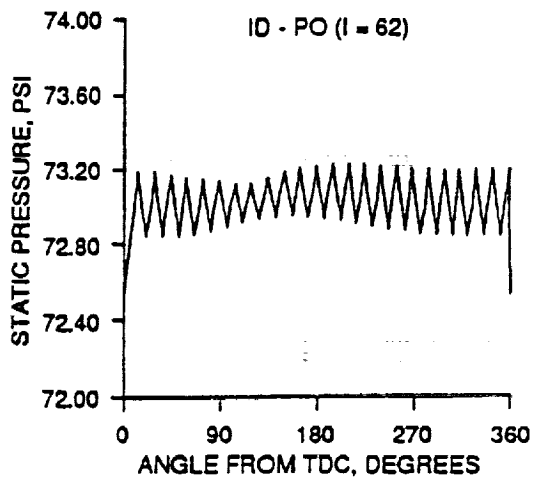
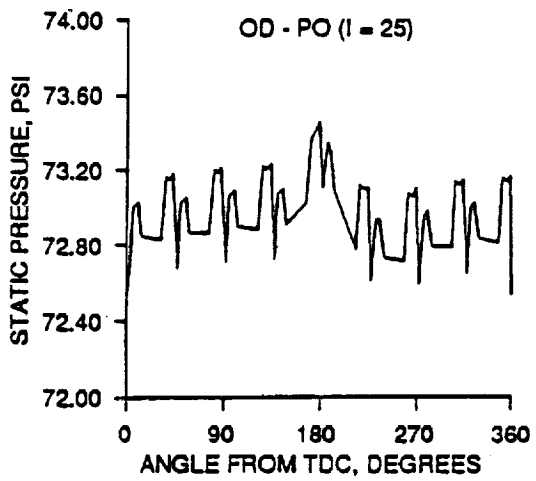
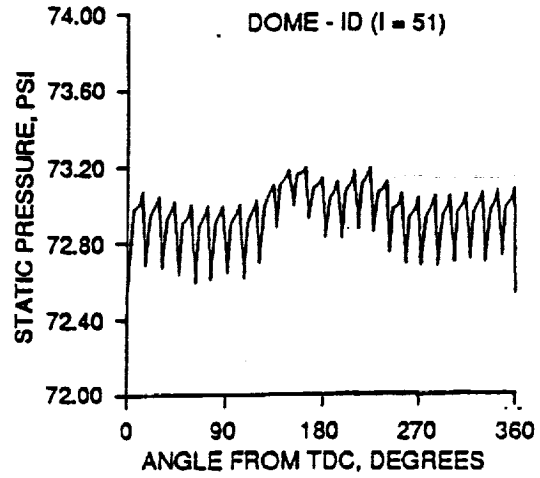
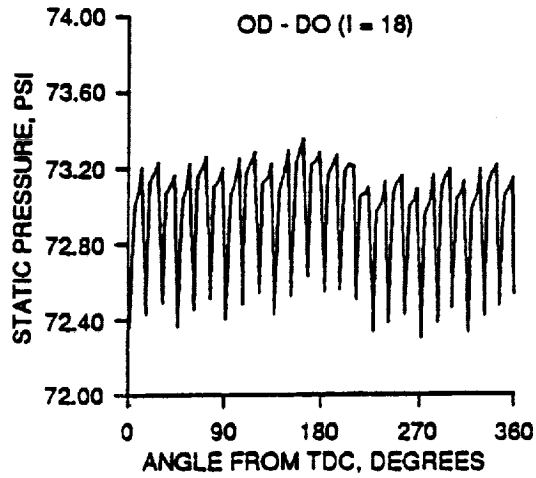
5. The fifth part of the document concludes by summarizing the key findings and recommendations. It stresses the importance of continuous monitoring and evaluation of the data management process to ensure it remains effective and aligned with the organization's goals.

significant effect on pressure distributions around the turbine plenum. The predicted results also show non-uniform pressure distributions on the bleed duct wall. The predicted results of non-uniform pressure distributions on the bleed duct wall (at  $I=43$  and  $J=20$ ) were compared to combustor rig test data in Figure 11. This comparison indicates model predictions agreed well with test data from combustor rig.

Having obtained good predictions of non-uniform pressure distribution on the bleed duct wall, it is then possible to consider another 3-D case run in order to study the effect of intergral bleed extraction on the pressure distributions around the combustor liner. Figures 12 and 13 show the predicted pressure distributions at various hole locations for a gas turbine combustor with and without an integral bleed. Comparison of Figures 12 and 13 confirms that integral bleed flow distribution has a great effect on the pressure distributions around the gas turbine combustor.



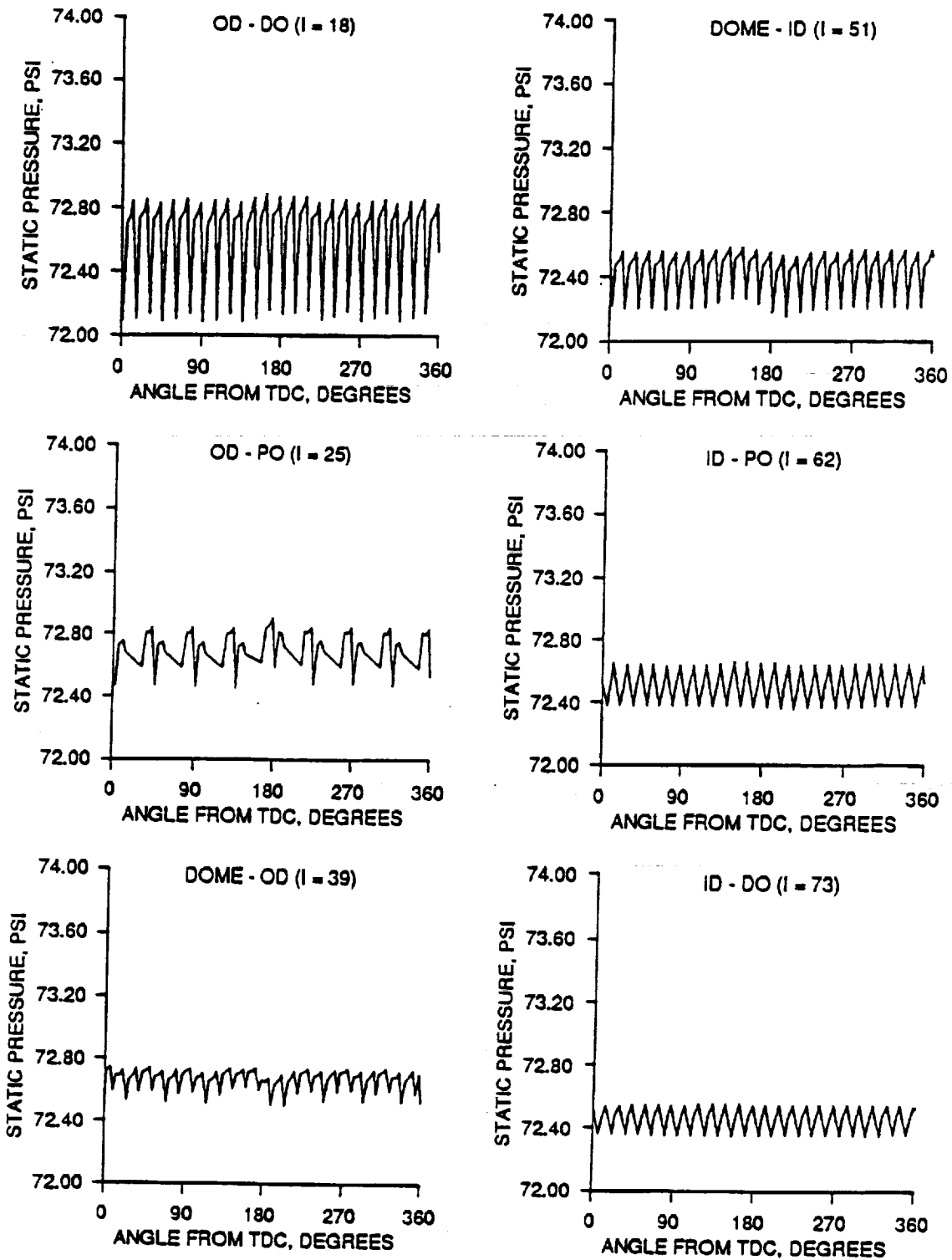
GC11476-11  
**Figure 11. Comparison of Predicted and Measured Pressure Distributions on the Bleed Duct Wall.**



GC11478-12

Figure 12. Predicted Pressure Distributions at Various Combustor Hole Locations.

C-5



GC11478-13

Figure 13. Predicted Pressure Distribution at Various Combustor Hole Locations (without Integral Bleed).

## CONCLUSIONS

An advanced 3-D CFD model based on a boundary-fitted, curvilinear, orthogonal grid system has been developed. The model is capable of predicting the complex external flow field of a gas turbine combustor with integral bleed. Several important findings from this study of Combustor-Integral Bleed flow interaction are summarized below:

(1) Integral bleed flow distribution has a great effect on the pressure distribution around the gas turbine combustor.

(2) The presence of atomizers and ignitors has a profound effect on pressure distribution around the combustor O.D. liner. Each atomizer or ignitor was found to be associated with a high pressure region upstream and a low pressure region downstream.

(3) The non-uniform pressure distribution usually causes non-uniform airflow distribution around the combustor liner and will result in hot and cold spots at the combustor exit.

(4) The recirculation zone formed near the annulus inlet has caused pressure loss near the combustor O.D. dilution holes. As a result, the dilution jet penetration is reduced and will result in high pattern factor at the combustor exit.

## REFERENCES

1. Thompson, J. F., 1982, "Numerical Grid Generation," North-Holland.
2. Spalding, D. B., 1972, "A Novel Finite Difference Formulation for Differential Expressions Involving Both First and Second Derivatives," Int. J. Num. Mech. Engr., Vol. 4, pp551.
3. Patankar, S. V., 1980, "Numerical Heat Transfer and Fluid Flow," McGraw-Hill-Hemisphere.
4. Przekwas, A. J., 1984, "Whole Field Solution Method for Elliptic Difference Equations with General Boundary Conditions," Numerical Heat Transfer, Vol-, pp-.
5. Roback, R. and Johnson, J. P., 1983, "Turbulent Confined Swirling Coaxial Jets," NASA CR-168252.
6. Sovran, G. and Klomp, E.G., 1967, "Experimentally Determined Optimum Geometries for Rectilinear Diffusers with Rectangular, Conical and Annular Cross Sections," Fluid Mechanics of Internal Flow, Elsevier, New York.

## ACKNOWLEDGEMENTS

The authors would like to thank Mr. Randy Williams for his encouragement of developing this 3-D Combustor-Integral Bleed Flow Interaction Model. They would also like to thank the AlliedSignal Engines management for permission to publish this paper.